Supporting Information for:

Hierarchically-Structured NiO Nanoplatelets as Mesoscale p-Type Photocathodes for Dye-Sensitized Solar Cells

*Cory J. Flynn,[†] EunBi E. Oh,[†] Shannon M. McCullough,[†] Robert W. Call,[‡] Carrie L. Donley,[§] Rene Lopez,[‡] and James F. Cahoon[†]**

[†]Department of Chemistry, University of North Carolina at Chapel Hill, Chapel Hill, NC 27599-3290, USA, [‡]Department of Physics and Astronomy, University of North Carolina at Chapel Hill, Chapel Hill, NC 27599-3255, USA, [§]Chapel Hill Analytical and Nanofabrication Laboratory (CHANL), Department of Applied Physical Sciences, University of North Carolina at Chapel Hill, Chapel Hill, NC 27599-3216, USA

*Corresponding Author
Email: jfcahoon@unc.edu

Supporting information includes:

Supplemental Figures S1-S11
Supplemental Table S1

SUPPORTING FIGURES

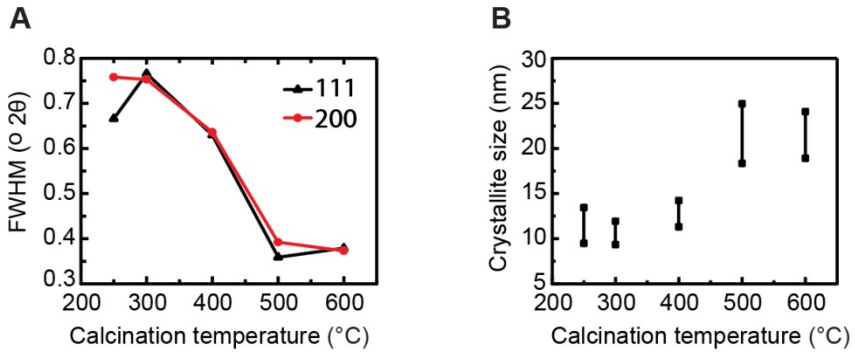

Figure S1. Temperature-dependent evolution of linewidths from powder XRD. (**A**) Full width at half maximum (FWHM) as a function of calcination temperature for the (111) reflection (black triangles and curve) and (200) reflection (red circles and curve). (**B**) Calculated crystallite size range from the Debye-Scherrer analysis utilizing a range of shape factors from 0.8-1.0.

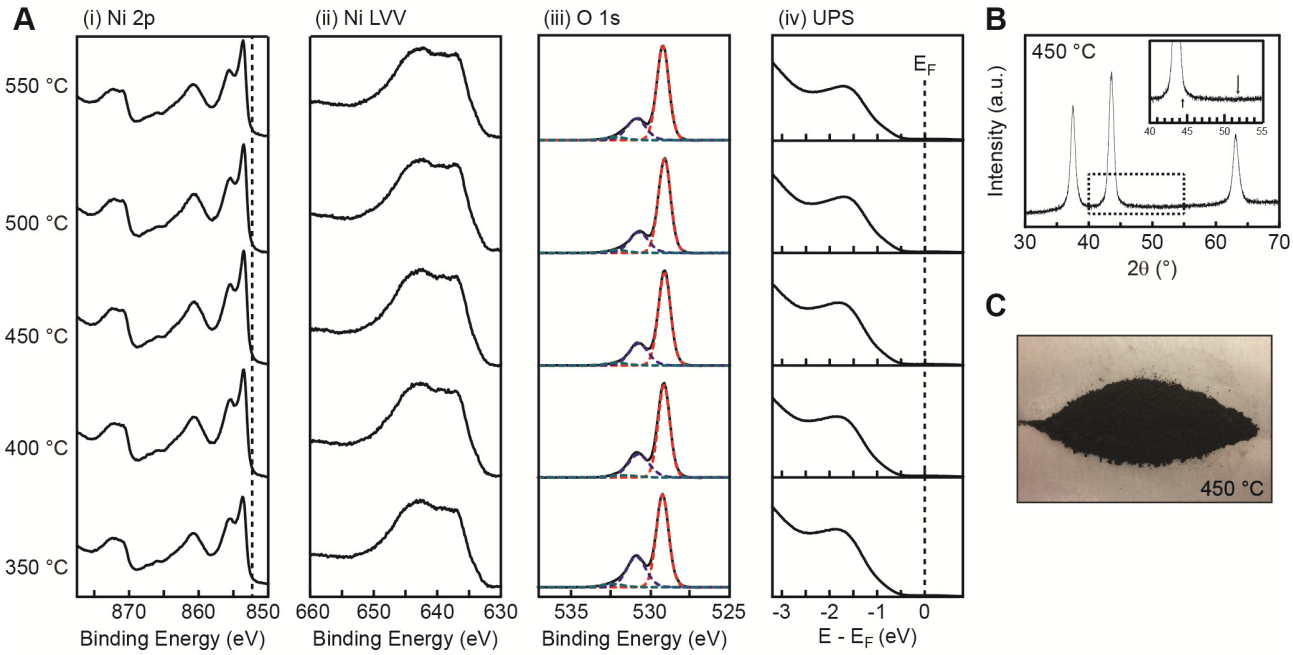

Figure S2. XPS, UPS, and XRD data of NiO nanoplatelets showing no evidence of metallic Ni^0. (**A**) (i) XPS spectra of the Ni 2p region typical of NiO. The absence of a peak 852.3 eV (black dashed line) and the presence of a peak at ~853.6 is indicative of NiO and not Ni^0.[1] (ii) XPS spectra of the Ni Auger region. The broad two-peak feature is similar to literature patterns indicative of NiO and not Ni^0. A single-broad peak would be expected for pure Ni^0.[2] (iii) XPS spectra of the O 1s region. Curves were fit to three Voigt functions centered at ~529.2, ~530.9, and ~531.6 eV, which correspond to octahedrally-coordinated oxygen in NiO (~529.2 eV) and under-coordinated oxygen in Ni_2O_3/NiOOH/$Ni(OH)_2$, (~530.9, ~531.6 eV). The area of the fits was used to determine a qualitative trend for the relative percentage of Ni in the two oxidation states, as detailed in Table S1.[2] (iv) UPS spectra of the valence band edge of NiO. The presence of Ni^0 would be shown as intensity up to the Fermi energy level marked with a black dashed line but is absent in all samples. (**B**) XRD spectra of NiO calcined at 450 °C. Inset: magnification of the region denoted by the black dashed box. Metallic Ni^0 would have additional peaks at the positions denoted by arrows in the inset, which are centered at 44.4 and 51.8° 2θ and are clearly absent from the spectra.[3] Spectra were obtained with a slower scan rate of 0.083° 2θ/minute rather than the typical 2° 2θ/minute. (**C**) Optical image of NiO calcined at 450 °C showing a deep-black color even with absence of Ni^0 in XRD and XPS/UPS spectra.

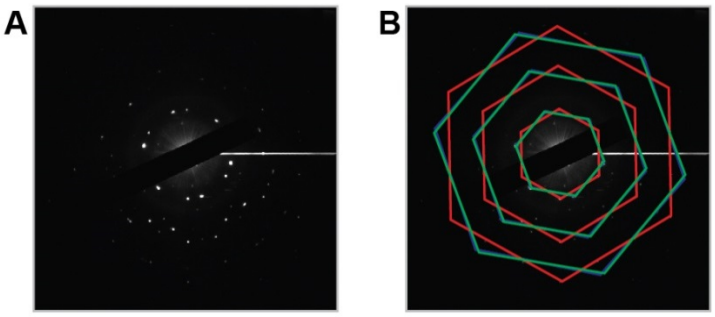

Figure S3. Twist grain boundaries in NiO. (**A**) SAED pattern of a NiO nanoplatelet calcined at 450 °C, showing evidence for twist grain boundaries (**B**) Hexagonal shapes overlaid in red, blue, and green to illustrate the twist grain boundaries apparent from the SAED pattern.

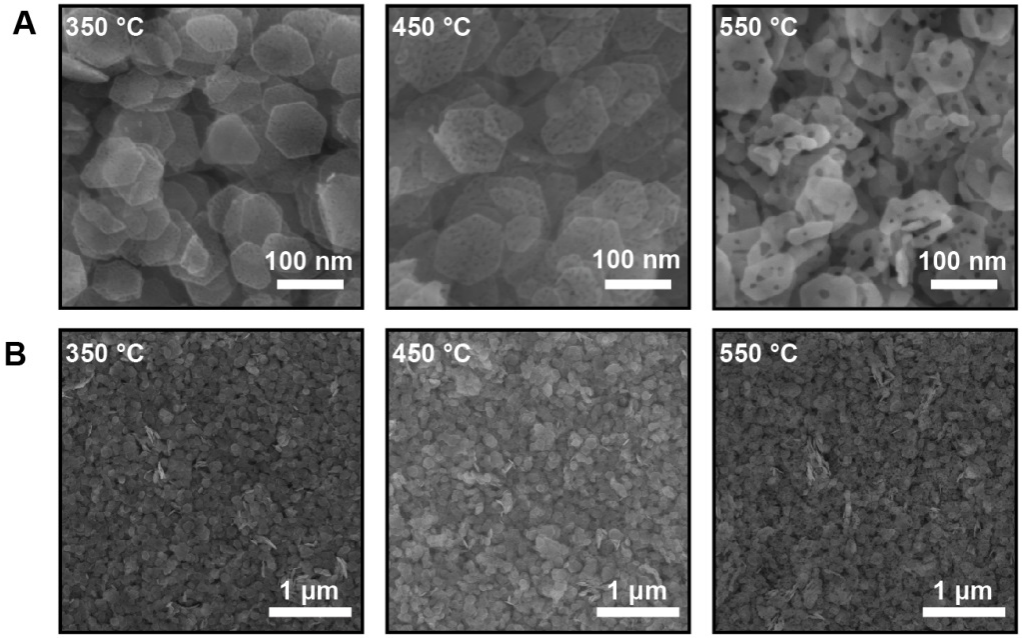

Figure S4. Morphology of the partially aligned mesoporous NiO Films. SEM images at high magnification (**A**) and low magnification (**B**) of NiO nanoplatelet mesoporous thin films annealed 350, 450, and 550 °C, from left to right, respectively. The films show partial alignment in the [111] direction, as evidenced by the large number of hexagonal (111) faces apparent in the images.

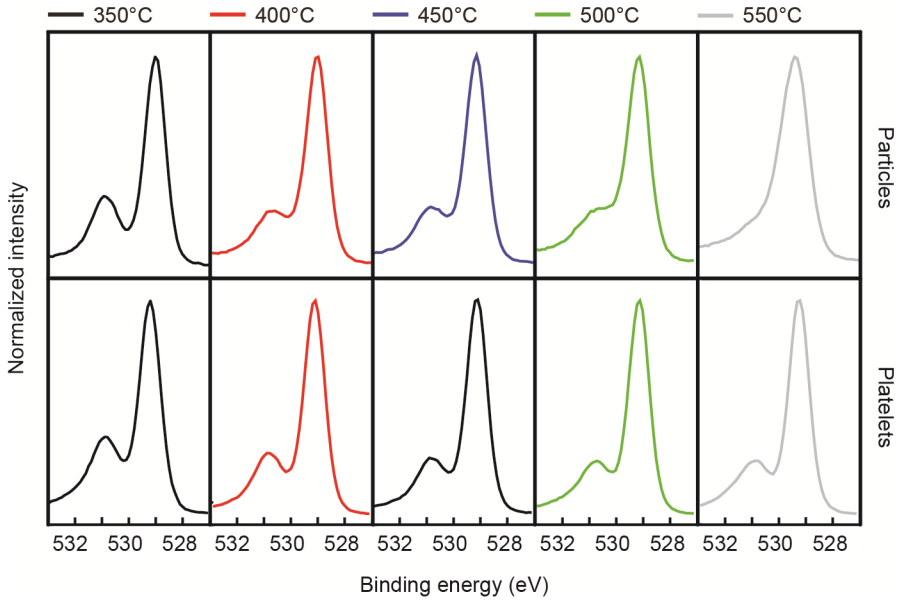

Figure S5. XPS spectra in the oxygen 1s region. Thin films annealed/calcined from 350 °C (far left) to 550 °C (far right) for nanoparticles (top) and nanoplatelets (bottom). All spectra are normalized. The peak at lower binding energy corresponds to octahedrally-coordinated oxygen in NiO (~529.2eV) whereas the peak at higher binding energy corresponds to under-coordinated oxygen in NiOOH/Ni_2O_3/$Ni(OH)_2$ (~530.9; ~531.6 eV).

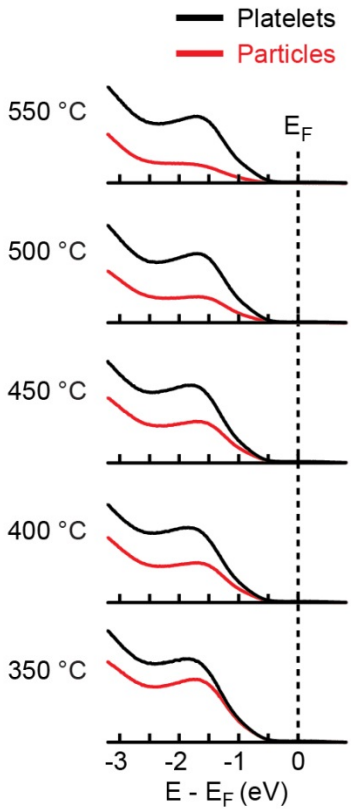

Figure S6. UPS measurements near the NiO valence band edge. UPS spectra for nanoplatelets (black) and nanoparticles (red) are shown as a function of the calcination/anneal temperature denoted to the left of each graph. The Fermi level, E_F, is denoted by the dashed black line. Extrapolation of the data sets at each temperature yields approximately equivalent differences between the valence band edge and Fermi level for particles and platelets at each temperature, indicating the doping level of the materials are approximately the same.

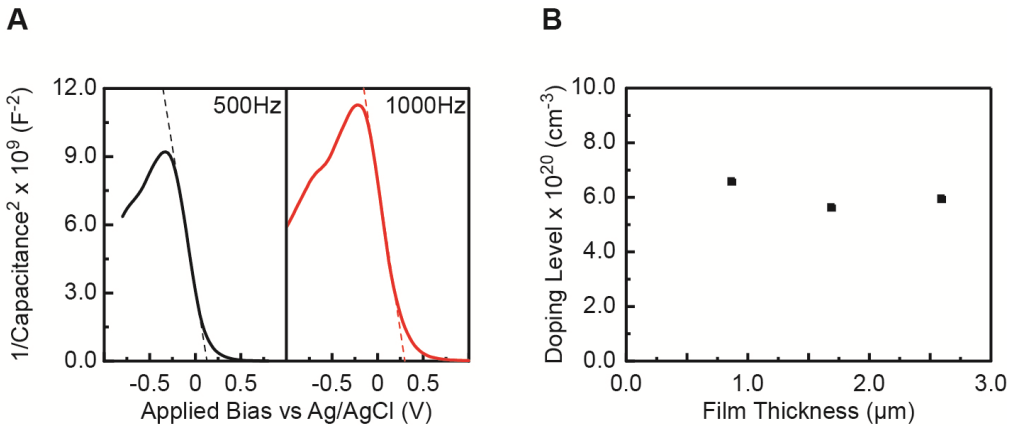

Figure S7. Mott-Schottky analysis of nanoplatelets calcined at 450 °C. (**A**) The capacitance determined from electrochemical impedance spectroscopy plotted in the form of the Mott Schottky Equation (Equation S1) for data acquired at an AC frequency of 500 Hz (black) and 1000 Hz (red). A linear fit to the linear portion of the decay (dashed lines) is shown with $R^2 >$ 0.98. The slope is converted to doping level using the projected area of the working electrode (A), the dielectric constant of NiO ($\varepsilon_R = 9.7$), the elementary charge q, and the permittivity of free space ε_0. (**B**) Doping determined from several thicknesses of NiO films with the same projected area. The doping level determined by Mott-Shottky analysis is independent of film thickness, justifying the use of projected area rather the surface area in the Mott-Schottky equation. However, the projected area most likely substantially underestimated the surface area giving rise to the capacitance measured in the Mott-Schottky analysis; thus, the doping level determined from this measurement represents an upper limit on the doping level.

$$\frac{1}{C^2} = \frac{2}{\varepsilon_0 \varepsilon_R A^2 q N_D}\left(V - V_{fb} - \frac{K_B T}{q}\right) \qquad \text{(Equation S1)}^4$$

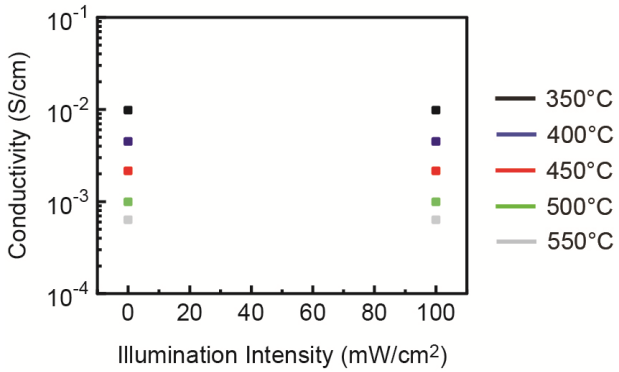

Figure S8. Photoconductivity of dyed NiO nanoplatelets. Measurements of the dark conductivity and 1-sun photoconductivity of NiO nanoplatelet thin films dyed with Coumarin-343 dye showing absence of a photoresponse. Experiments were also performed by directly pumping the dye with the output of 405 nm continuous-wave laser and still showed no photoresponse for illumination intensities of up to ~100 mW/cm^2.

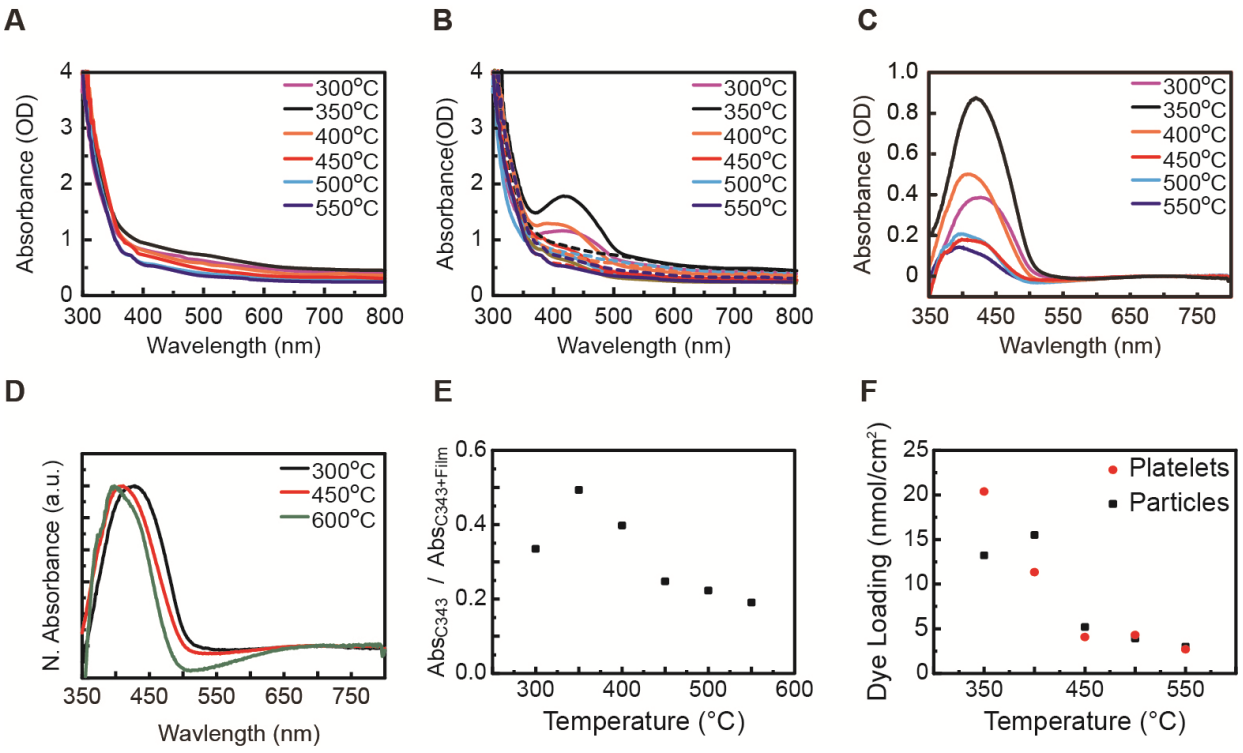

Figure S9. Absorption in NiO films with and without Coumarin-343. (**A**) Absorbance of un-dyed NiO films for a range of calcination temperatures (**B**) Absorbance of dyed NiO films (solid curves) for a range of calcination temperatures. The absorbance curves for the same un-dyed films are plotted as dashed lines. (**C**) Absorbance of Coumarin-343 adsorbed on the NiO surface plotted by taking the difference spectra between the dyed and un-dyed films for a range of calcination temperatures with background correction at 700 nm. (**D**) Normalized absorbance spectra of Coumarin-343 adsorbed on NiO films calcined at 300 (black), 450 (red), and 600 °C (green). (**E**) Fraction of the dye absorption relative to the total absorption of a dye-loaded NiO film. This fraction does not follow the same trend as J_{SC}, indicating that the background absorption from the NiO material is not a dominant factor in determining the overall trend in J_{SC} with temperature. (**F**) Calculated dye loading of platelets (black squares) and particles (red circles) with Coumarin 343 as a function of calcination/annealing temperature.

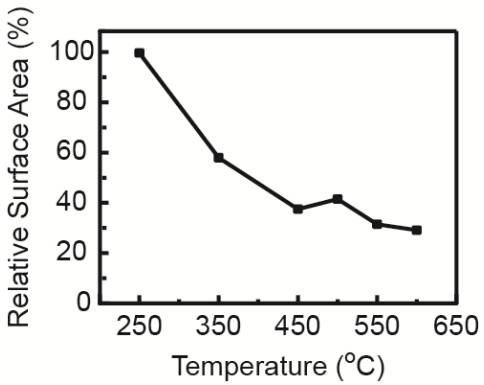

Figure S10. Surface area of NiO films as a function of calcination temperature. BET determination of the surface area for loose NiO powders calcined at temperatures ranging from 250-600 °C. Values are relative because of the large potential for error in BET measurements of these materials.

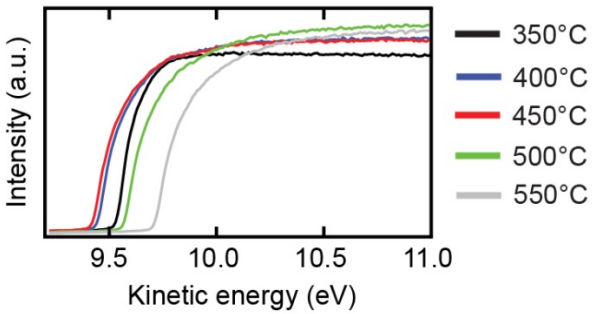

Figure S11. Temperature-dependent NiO nanoplatelet work function from UPS measurements near the secondary electron cut-off. UPS spectra collected for calcination temperatures ranging from 350 to 550 °C were fit to a line in the range around ~9.5 eV to determine the work function as a function of temperature from the intercept with baseline.

Table S1. Areas under the curve as derived from Voigt fits to the O 1s XPS spectra

	Nanoplatelet				
	350 °C	***400 °C***	***450 °C***	***500 °C***	***550 °C***
~529.2 NiO	64.1	66.6	70.7	72.4	71.4
~530.9 NiOOH; Ni_2O_3; $Ni(OH)_2$	32.2	30.1	25.8	24.3	24.9
~531.6 NiOOH; Ni_2O_3; $Ni(OH)_2$	3.7	3.3	3.5	3.6	3.7
	Nanoparticle				
	350 °C	***400 °C***	***450 °C***	***500 °C***	***550 °C***
~529.2 NiO	66.9	73.2	70.5	67.9	77.4
~530.9 NiOOH; Ni_2O_3; $Ni(OH)_2$	29.7	24.3	26.0	28.1	19.4
~531.6 NiOOH; Ni_2O_3; $Ni(OH)_2$	3.3	2.5	3.4	3.9	3.2

REFERENCES

(1) Wagner, C. D.; Muilenberg, G. E., *Handbook of x-ray photoelectron spectroscopy: a reference book of standard data for use in x-ray photoelectron spectroscopy*. Physical Electronics Division, Perkin-Elmer Corp.: 1979.

(2) Ratcliff, E. L.; Meyer, J.; Steirer, K. X.; Garcia, A.; Berry, J. J.; Ginley, D. S.; Olson, D. C.; Kahn, A.; Armstrong, N. R. Evidence for near-Surface NiOOH Species in Solution-Processed NiOx Selective Interlayer Materials: Impact on Energetics and the Performance of Polymer Bulk Heterojunction Photovoltaics. *Chemistry of Materials* **2011,** *23*, 4988-5000.

(3) Zhu, H.; Hagfeldt, A.; Boschloo, G. Photoelectrochemistry of Mesoporous NiO Electrodes in Iodide/Triiodide Electrolytes. *The Journal of Physical Chemistry C* **2007,** *111*, 17455-17458.

(4) Gelderman, K.; Lee, L.; Donne, S. W. Flat-Band Potential of a Semiconductor: Using the Mott–Schottky Equation. *Journal of Chemical Education* **2007,** *84*, 685.